Importance of Ligand Effect in Selective Hydrogen Formation via Formic Acid Decomposition on the Bimetallic Pd/Ag Catalyst from First-Principles

ARTICLE *in* THE JOURNAL OF PHYSICAL CHEMISTRY C · OCTOBER 2014

Impact Factor: 4.77 · DOI: 10.1021/jp5050817

8 AUTHORS, INCLUDING:

Hyung Chul Ham
Korea Institute of Science and Technology
48 PUBLICATIONS **289** CITATIONS

SEE PROFILE

THE JOURNAL OF PHYSICAL CHEMISTRY C

Article

pubs.acs.org/JPCC

Importance of Ligand Effect in Selective Hydrogen Formation via Formic Acid Decomposition on the Bimetallic Pd/Ag Catalyst from First-Principles

Jinwon Cho,[†,‡] Sangheon Lee,[†] Jonghee Han,[†,‡] Sung Pil Yoon,[†] Suk Woo Nam,[†,‡] Sun Hee Choi,[†] Kwan-Young Lee,[‡] and Hyung Chul Ham*[,†,§]

[†]Fuel Cell Research Center, Korea Institute of Science and Technology (KIST), Hwarangno 14-gil 5, Seongbuk-gu, Seoul, 136-791, Republic of Korea

[§]Clean Energy and Chemical Engineering, University of Science and Technology (UST), 217 Gajungro, Yuseong-gu, Daejeon, 305-333, Republic of Korea

[‡]Green School (Graduate School of Energy and Environment), Korea University, 145, Anam-ro, Seongbuk-gu, Seoul 136-701, Republic of Korea

Supporting Information

ABSTRACT: The critical role of the Ag−Pd ligand effect (which is tuned by changing the number of Pd atomic layers) in determining the dehydrogenation and dehydration of HCOOH on the bimetallic Pd/Ag catalysts was elucidated by using the spin-polarized density functional theory (DFT) calculations. Our calculations suggest that the selectivity to H_2 production from HCOOH on the bimetallic Pd/Ag catalysts strongly depends on the Pd atomic layer thickness at near surface. In particular, the thinnest Pd monolayer in the Pd/Ag system is responsible for enhancing the selectivity of HCOOH decomposition toward H_2 production by reducing the surface binding strength of specific intermediates such as HCOO and HCO. The dominant Ag−Pd ligand effect by the substantial charge donation to the Pd surface from the subsurface Ag [which significantly reduce the density of state (particularly, $d_{z^2-r^2}$ orbital) near the Fermi level] proves to be a key factor for the selective hydrogen production from HCOOH decomposition, whereas the expansive (tensile) strain imposed by the underlying Ag substrate plays a minor role. This work hints on the importance of properly engineering the surface activity of the Ag−Pd core−shell catalysts by the interplay between ligand and strain effects.

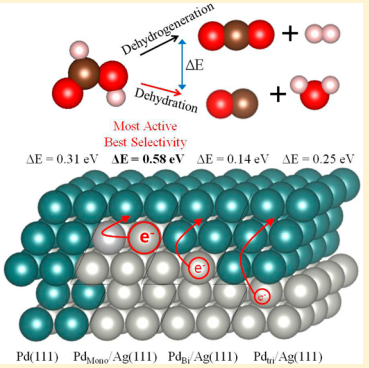

1. INTRODUCTION

Formic acid (HCOOH) is considered as one of the most promising compounds for chemical hydrogen (H_2) storage, particularly for low-temperature fuel cell applications.[1] HCOOH readily decomposes into H_2 and CO_2 in the presence of a suitable catalyst.[2] The decomposition of HCOOH also includes a side reaction, yielding H_2O and CO.[3] At elevated reaction temperatures, both product groups can be interconnected via the water−gas shift reaction, resulting in an increase of CO concentration.[4] The gas stream from the decomposition of HCOOH has to be free from CO gas (<10 ppm), or the catalytic performance of the fuel cells will be significantly degraded due to the contamination of electrodes by CO.[5] Therefore, catalysts that are highly selective (suppressing the formation of CO) and active at low temperatures for the decomposition of HCOOH into H_2 and CO_2 are indispensable to realize HCOOH-based low-temperature fuel cells.[6]

There have been reports of excellent catalytic activities for the decomposition of HCOOH using homogeneous catalysts at ambient temperatures.[3] In this case, however, the separation issues and the use of organic solvents lead to severe difficulties in H_2 production device fabrication.[7] Heterogeneous catalysts are free from these issues, but their activity and selectivity are known to be lower than the homogeneous catalysts.[8] Recent experimental studies of heterogeneous catalysts using advanced nanoparticle synthesis have shown promising results.[1a,9] In particular, Tedsree et al. investigated the rate of HCOOH decomposition over multiple metal−Pd (M−Pd) core−shell catalysts and reported a Ag-Pd core−shell catalyst, among the M-Pd catalysts investigated, as the most active catalyst for H_2 production from HCOOH decomposition at room temperature.[9] In the case of Ag−Pd core−shell catalyst, nearly 100% conversion of HCOOH was achieved for longer reaction time, while the CO_2/H_2 was found close to unity and no CO was generated. In addition, the Pd shell of Pd-based nanoparticle was fully encapsulating the metal core, and the core−shell structure proved to be stable under reaction conditions with no evidence of migration of metal core to surface in the case of Ag−Pd core−shell catalysts. The enhanced catalytic activities of

Received: May 23, 2014
Revised: August 24, 2014
Published: September 4, 2014

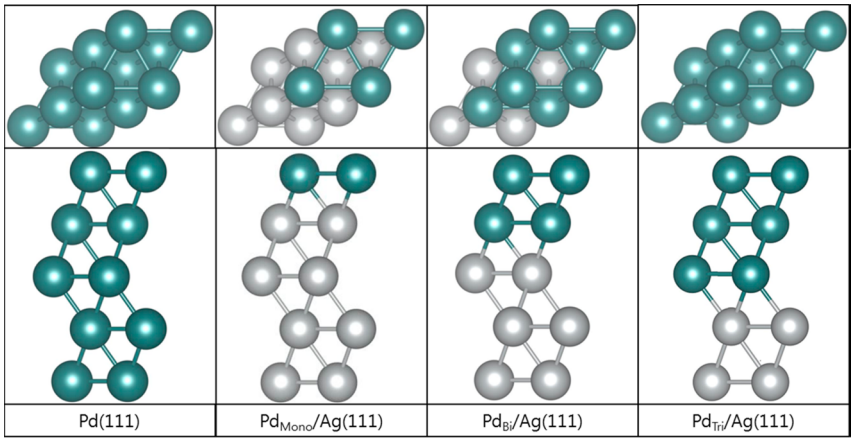

Figure 1. Top (the upper row) and side (the lower row) views of the structures modeled in this study. From left, they are the pure Pd surface[Pd(111)], Pd monolayer supported on the Ag(111) substrate [Pd_{Mono}/Ag(111)], Pd bilayer on the Ag(111) substrate [Pd_{Bi}/Ag(111)], and Pd trilayer on the Ag(111) substrate [Pd_{Tri}/Ag(111)]. Pd and Ag atoms are shown in green and gray, respectively.

the Ag−Pd core−shell system can be attributed to the electronic promotion of the surface Pd atoms by Ag or the lattice mismatch between Ag and Pd. However, the underlying principles that govern the HCOOH decomposition in Ag−Pd core−shell system still remained unclear.

In this work, we present the influence of Pd atomic layer thickness in the bimetallic Pd/Ag system on the productivity and selectivity to H_2 production from HCOOH decomposition to get a detailed theoretical understanding of the origin of enhanced catalytic activities of the Ag−Pd core−shell system (especially, the important role of ligand effect). In addition, we perform the electronic structure analysis on each Pd/Ag surface to elucidate the relative contribution of the different alloying effects embedded in the bimetallic Pd/Ag system to catalysis.

2. THEORETICAL DETAILS

The calculations reported herein were performed on the basis of spin polarized density functional theory (DFT) within the revised Perdew−Burke−Ernzerhof (rPBE) functional, as implemented in the Vienna Ab Initio Simulation Package (VASP).[10] The projector augmented wave (PAW) method with a planewave basis set was employed to describe the interaction between ion cores and valence electrons.[11] An energy cutoff of 350 eV was applied for expansion of the electronic eigenfunctions. For the Brillouin zone integration,[12] we used a (5 × 5 × 1) Monkhorst−Pack mesh of *k*-points to determine the optimal geometries and total energies of systems. For the electronic structure calculation, we increase the *k*-point mesh to (12 × 12 × 1). Reaction pathways and barriers were determined using the climbing-image nudged elastic band method (c-NEBM)[13] for each elementary step.

For the pure Pd and bimetallic Pd/Ag model surfaces, we constructed a supercell slab of a face-centered cubic (FCC) (111) surface that consists of a hexagonal 2 × 2 surface unit cell with five atomic layers, each of which contains four atoms. As illustrated in Figure 1, four-different surfaces were constructed for the pure Pd surface [indicated by Pd(111)], Pd monolayer supported on the Ag(111) substrate [Pd_{Mono}/Ag(111)], Pd bilayer on the Ag(111) substrate [Pd_{Bi}/Ag(111)], and Pd trilayer on the Ag(111) substrate [Pd_{Tri}/Ag(111)]. The Pd/Ag model surfaces correspond to the experimental observation that the Pd shell of the Pd-based nanoparticle fully encapsulates the Ag metal core.[9]

The slab is separated from its periodic images in the vertical direction by a vacuum space corresponding to seven atomic layers. While the bottom two layers of the five-layered slab are fixed at corresponding bulk positions, the upper three layers are fully relaxed using the conjugate gradient method until residual forces on all the constituent atoms become smaller than 5 × 10^{-2} eV/Å. The lattice constant for bulk Pd is predicted to be 4.00 Å, which is virtually identical to the previous calculations.[14]

The adsorption energy (E_{ad}) of a species M on a surface are determined via $E_{ad} = |E_{surf} + E_M| - |E_{M*}|$, where E_{M*} and E_{surf} are the total energies of the surface with and without the adsorbed M, respectively, and E_M is the total energy of the species M in the vacuum, and $|x|$ indicates the absolute value of x.

3. RESULTS AND DISCUSSION

3.1. Effect of Pd Atomic Layer Thickness on the Dehydrogenation of HCOOH. It has been generally accepted that the oxidation of HCOOH on Pd and other noble metal catalysts proceeds through a dual-path mechanism,[15] which is consisted of the dehydrogenation and dehydration path. In dehydrogenation path, HCOOH is oxidized to form H_2 and CO_2 (HCOOH → H_2 + CO_2). According to a number of experimental and theoretical reports,[6,9,16] the formate (HCOO; which is linked to a bridge site by its two oxygen atoms on the catalytic surface) is believed to be a viable intermediate in the dehydrogenation pathway. On the other hand, in dehydration path, CO and H_2O are produced from HCOOH decomposition (HCOOH → CO + H_2O) through the formation of formyl (HCO) or carbonyl (COOH) intermediates.[6,17] A recent DFT study has shown that the dehydration reaction via HCO is kinetically more favorable than that via COOH species.[6] For the CO-free H_2 production from HCOOH, the catalytic system should be designed to enhance the reaction rate for dehydrogenation reaction while suppressing the dehydration reaction.

In this work, we investigated the reaction energetics/barriers for the dehydrogenation and dehydration steps (see Figure 2) on the pure Pd and bimetallic Pd/Ag model surfaces by changing the atomic layer thickness at near surface to understand the importance of ligand effect in determining the selectivity of HCOOH decomposition toward H_2 production; for dehydrogenation pathway, (D1) the first dehydrogenation

dx.doi.org/10.1021/jp5050817 | J. Phys. Chem. C 2014, 118, 22553−22560

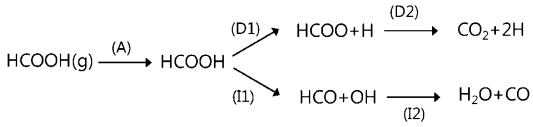

Figure 2. Schematic illustration of the dehydrogenation and dehydration steps for HCOOH oxidation considered in this study; The decomposition reaction proceeds via the adsorption of HCOOH to the Pd surface, followed by: for direct steps, (D1) the first dehydrogenation from HCOOH via the O−H cleavage [HCOOH → HCOO + H] and (D2) the second dehydrogenation from HCOO via the C−H cleavage [HCOO → CO_2 + H], and for indirect steps, (I1) the decomposition of HCOOH via the C−O cleavage, yielding HCO and OH [HCOOH → HCO + OH], and (I2) the formation of CO and H_2O by the combination reaction of OH and HCO [HCO + OH → CO + H_2O].

from HCOOH via the O−H cleavage [HCOOH → HCOO + H], (D2) the second dehydrogenation from HCOO via the C−H cleavage [HCOO → CO_2 + H]; for dehydration pathway, (I1) the decomposition of HCOOH via the C−O cleavage, yielding HCO and OH [HCOOH → HCO + OH], (I2) the formation of CO and H_2O by the combination reaction of OH and HCO [HCO + OH → CO + H_2O].

Figure 3 depicts two selective HCOOH decomposition pathways over the $Pd_{Mono}/Ag(111)$ surface, while the

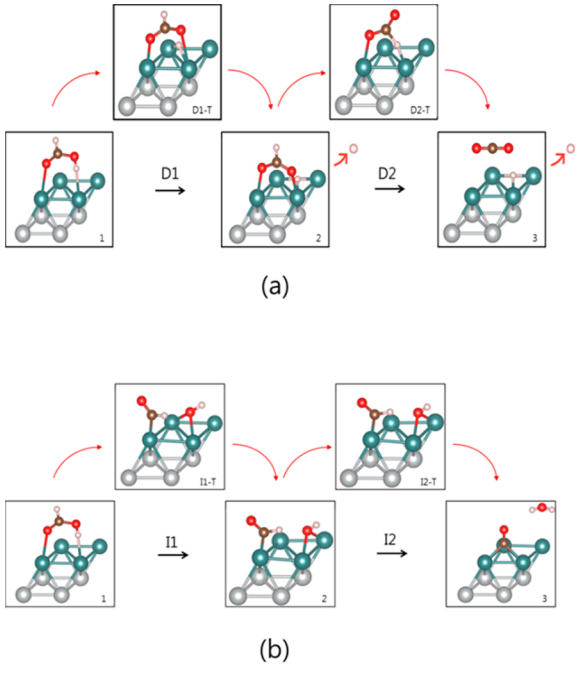

Figure 3. Two selective HCOOH decomposition pathways of $Pd_{Mono}/Ag(111)$. Dehydrogenation pathway to HCOO + H then to CO_2 + H_2 is indicated as D1 and D2, and the dehydration pathway to CO + H_2O via the intermediate state HCO + OH is labeled as I1 and I2. The HCOOH decomposition pathways of $Pd_{Bi}/Ag(111)$, $Pd_{Tri}/Ag(111)$, pure Pd(111), and $Pd(111)_{Str}$ are shown in Supporting Information. The green balls represent the surface of Pd, and the brown, red, and white balls represent C, O, and H atoms, respectively.

corresponding potential energy diagrams are shown in Figure 4. For these selective pathways, Table 1 summarizes the calculated total energy changes (ΔE) and activation barriers (E_a) for the dehydrogenation and dehydration reactions on five different Pd surfaces [Pd(111), $Pd_{Mono}/Ag(111)$, Pd_{Bi}/Ag-

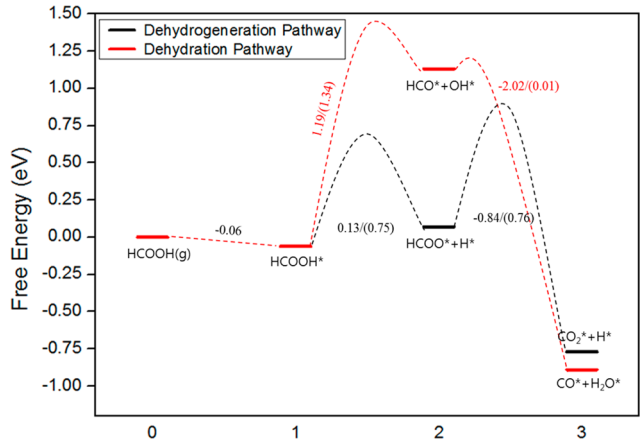

Figure 4. Predicted potential energy diagram for the HCOOH decomposition on the $Pd_{Mono}/Ag(111)$ via the dehydrogenation and dehydration pathways. The calculated total energy changes and energy barriers in parentheses are shown in the graph where the black line represents the dehydrogenation pathway and the red line represents the dehydration pathway. See the Supporting Information for the potential energy diagram of $Pd_{Bi}/Ag(111)$, $Pd_{Tri}/Ag(111)$, pure $Pd(111)_{Str}$, and pure Pd(111) cases.

(111), $Pd_{Tri}/Ag(111)$, and $Pd(111)_{Str}$]. Here, the $Pd(111)_{Str}$ indicates the 5.8% expansively strained Pd(111) surface where the effect of the heterometallic interaction (interatomic mixing between Ag and Pd) in the Pd/Ag system on the catalytic activity of surface Pd atoms is almost eliminated but the effect of surface lattice strain is still maintained. The results clearly show that the selectivity in the decomposition of HCOOH on Pd and Pd/Ag catalysts are strongly affected by the number of Pd atomic layers on the Ag substrate. Next, we make a detailed analysis of each reaction step.

First, for five different Pd surfaces we find that the HCOOH molecule weakly binds at the top site of two Pd atoms (which is linked to the oxygen of C═O and hydrogen of O−H in HCOOH, respectively) with the adsorption energy of 0.06−0.08 eV. Next, for the first dehydrogenation reaction [(D1) HCOOH → HCOO + H], our calculations predict the substantially higher exothermicity on the $Pd_{Bi}/Ag(111)$ (ΔE = −0.43 eV), $Pd_{Tri}/Ag(111)$ (ΔE = −0.25 eV), and $Pd(111)_{Str}$ (ΔE = −0.24 eV) surfaces than the pure Pd(111) surface (ΔE = 0.01 eV), but on the $Pd_{Mono}/Ag(111)$ surface, the reaction energetic for D1 is calculated to be endothermic by 0.13 eV. Correspondingly, the barrier for step D1 decreases from 0.69 eV [Pd(111)] to 0.45 eV [$Pd_{Bi}/Ag(111)$], to 0.58 eV [$Pd_{Tri}/Ag(111)$], and to 0.58 eV [$Pd(111)_{Str}$], but increases to 0.75 eV [$Pd_{Mono}/Ag(111)$]. Looking at the second dehydrogenation reaction [(D2) HCOO → CO_2 + H], however, the Pd monolayer on the Ag substrate [$Pd_{Mono}/Ag(111)$] turns out to be energetically most favorable (ΔE = −0.68 eV [Pd(111)], −0.84 eV [$Pd_{Mono}/Ag(111)$], −0.56 eV[$Pd_{Bi}/Ag(111)$], −0.63 eV [$Pd_{Tri}/Ag(111)$], and −0.65 eV [$Pd(111)_{Str}$]) and in turn have the lowest barrier compared to the pure Pd(111), $Pd_{Bi}/Ag(111)$, and $Pd_{Tri}/Ag(111)$cases (Note the order of barriers for step D2:0.85 eV [Pd(111)] ≈ 0.83 eV [$Pd_{Tri}/Ag(111)$] ≈ 0.84 eV [$Pd_{Bi}/Ag(111)$] ≈ 0.84 eV [$Pd(111)_{Str}$] > 0.76 eV [$Pd_{Mono}/Ag(111)$]). Modification of the reaction energy and barrier as a result of a change in thickness of the Pd overlayer indicates that the number of Pd atomic layers on Ag substrate plays an important role in determining the dehydrogenation reaction rate. Assuming that an elementary step with the lowest

dx.doi.org/10.1021/jp5050817 | J. Phys. Chem. C 2014, 118, 22553−22560

Table 1. Calculated Total Energy Changes (ΔE) and Activation Barriers (E_a in parentheses) for Dehydrogenation and Dehydration Steps on the Pure Pd and Pd/Ag Catalysts[a]

$\Delta E/(E_a)$	$Pd_{Mono}/Ag(111)$	$Pd_{Bi}/Ag(111)$	$Pd_{Tri}/Ag(111)$	$Pd_{Str}/(111)$	Pd(111)
(D1) HCOOH to HCOO + H	0.13/(0.75)	−0.43/(0.45)	−0.25/(0.58)	−0.24/(0.58)	0.01/(0.69)
(D2) HCOO to CO_2 + H	−0.84/(0.76)	−0.56/(0.84)	−0.63/(0.83)	−0.65/(0.84)	−0.68/(0.85)
(I1) HCOOH to HCO + OH	1.19/(1.34)	0.57/(0.98)	0.68/(1.08)	0.78/(1.11)	0.97/(1.16)
(I2) HCO + OH to CO and H_2O	−2.02/(0.01)	−1.71/(0.25)	−1.85/(0.03)	−1.75/(0.17)	−1.79/(0.07)

[a]The values are given in eV.

reaction energy barrier is taken as the rate-determining elementary step, we take the step D2 as the rate-determining step over all Pd surfaces we considered. This is also well supported by a previous experimental study which suggested that the decomposition of the surface formate species probably being a rate-determining step.[18] Comparing the barriers in a rate-determining step, we find that the $Pd_{Mono}/Ag(111)$ surface can greatly enhance the reaction rate in dehydrogenation pathway compared to the Pd (111) surface case, while for the $Pd_{Bi}/Ag(111)$, $Pd_{Tri}/Ag(111)$, and $Pd(111)_{Str}$ surfaces, the improvement is insignificant [Here, we performed additional calculations over 3 × 3 periodic Pd/Ag(111) slab structures (corresponding to 1/9 monolayer coverage) and compared the results with the results over the 2 × 2 periodic Pd/Ag(111) slab structures (corresponding to 1/4 monolayer coverage), indicating that the two cases were found to exhibit similar trends]. This would be consistent with a recent experimental study where the highest activity of the Ag−Pd core−shell catalysts toward the HCOOH decomposition is achieved when the Pd shell thickness is the thinnest.[9] In particular, the Pd monolayer on the Ag substrate would be crucial for notably enhancing the kinetics of dehydrogenation of HCOOH.

3.2. Effect of Pd Atomic Layer Thickness on the Dehydration of HCOOH. For the [(I1) HCOOH → HCO + OH] and [(I2) HCO + OH → CO + H_2O] reactions, our calculation shows that the barriers for step I1 (0.98−1.34 V) are considerably higher than the barriers for step I2 (0.01−0.25 eV) for four different Pd surfaces, suggesting that once the scission of C−O bond in HCOOH (step I1) is activated, the following combination reaction of OH and HCO (step I2) can occur more easily (thus, the step I1 is considered to be a rate-determining step in dehydration pathway we considered). Looking closely at the rate-determining step (I1), the Pd monolayer substantially increases the endothermcity (ΔE = 1.19 eV) and barrier (E_a = 1.34 eV) compared to the pure Pd (111) surface (ΔE = 0.97 eV, E_a = 1.16 eV), while the opposite is true for the Pd bilayer, Pd trilayer, and strained surfaces (ΔE = 0.57 eV and E_a = 0.98 eV for $Pd_{Bi}/Ag(111)$; ΔE = 0.68 eV and E_a = 1.08 eV for $Pd_{Tri}/Ag(111)$; ΔE = 0.78 eV, E_a =1.18 eV for $Pd(111)_{Str}$).

Expecting that the barrier variation of a rate-determining step between dehydrogenation and dehydration reaction is related to the selectivity in formic acid oxidation, we also compared the activation barrier difference (ΔE_a): ΔE_a = 0.27 eV, [$Pd(111)_{Str}$)], 0.25 eV [$Pd_{Tri}/Ag(111)$], 0.14 eV [$Pd_{Bi}/Ag(111)$], 0.58 eV [$Pd_{Mono}/Ag(111)$], 0.31 eV [Pd(111)], indicating that the $Pd_{Mono}/Ag(111)$ case greatly enhances the selectivity to dehydrogenation route, while for the $Pd_{Bi}/Ag(111)$, $Pd_{Tri}/Ag(111)$, and $Pd(111)_{Str}$ cases the opposite is true. These clearly state that the Pd atomic layer thickness is a key factor in designing the bimetallic Pd/Ag catalysts, and it should be as thin as one atomic layer to maximally achieve the enhanced reactivity and selectivity toward the dehydrogenation of HCOOH.

3.3. Strain versus Ligand Effect in Pd/Ag Catalysts. To better understand the role of Pd atomic layer thickness in enhancing the dehydrogenation of HCOOH, we further examined how the different alloying effects embedded in the bimetallic Pd/Ag catalyst affects the surface adsorption energies of key intermediates generated during the HCOOH decomposition. Two alloying mechanisms can be mainly related to the variation in the catalytic activity of the bimetallic Pd/Ag catalyst. That is, the activity of surface Pd atoms are not only modified by the mismatch of lattice parameters between Pd and Ag (the so-called strain effect[20]), but also by the electronic structure change due to the Pd−Ag interaction [the so-called electronic (ligand) effect[8b,21]]. To understand the relative role of each alloying effect, we attempt to decouple the Ag substrate strain effect from the Pd−Ag electronic (ligand) effect by calculating the adsorption energy (E_{ad}) of key intermediates on the 5.8% expansively strained Pd(111) surface [$Pd_{str}(111)$; Note that the lattice constant of Ag is considerably greater by 5.8% than that of Pd and thus the surface Pd atoms are under a significant expansive strain imposed by the underlying Ag substrate]. Here, the E_{ad} for the $Pd_{str}(111)$ case can represent the contribution of strain effect to the adsorption energy of intermediates on the surface (excluding the ligand contribution). In Table 3, for the HCOO, H, HCO, CO, and OH, we find the increase of adsorption energy by 0.04−0.15 eV on the $Pd_{str}(111)$ surface compared to the pure Pd(111) case, implying that the surface expansive strain imposed by the underlying Ag substrate in the $Pd_{Mono}/Ag(111)$ and $Pd_{Bi}/Ag(111)$ surfaces tends to increase the adsorption energy of key intermediates. This is also supported by the calculation of surface electronic structures: the local density of states (LDOS) projected onto the *d* states of surface Pd atoms, as shown in Figure 5. For the $Pd_{str}(111)$ case, as expected, our calculation predict the upshift of the *d* band (the increase of average energy of the *d* band) and the increase of the LDOS near the Fermi level (-0.5 eV $< E - E_f < 0$ eV) compared to the pure Pd(111) case. Note that the expansive (tensile) strain tends to move up the *d* band toward Fermi level and in turn strengthen the interaction of surface atoms with various adsorbates.[20,22]

Next, in order to understand the relative ligand contribution of the Ag(substrate)−Pd(surface) interaction to the adsorption energy of intermediates, we calculate the difference in the surface adsorption energy of intermediates between Pd/Ag and strained Pd surfaces [indicated by ΔE_{ligand}, which is defined as $E_{ad}(Pd/Ag) - E_{ad}(Pd_{Str})$], as summarized in Table 2. For the $Pd_{Mono}/Ag(111)$ case, we predict the negative values of Ag−Pd ligand contribution for all intermediates [ΔE_{ligand} = −0.29 eV (HCOO), −0.26 eV(HCO), −0.16 eV(OH), −0.13 eV(CO), and −0.09 eV (H)], suggesting that the Ag−Pd ligand effect acts in a direction to lower the adsorption energy, which is the opposite direction of expansive strain (increase the adsorption

dx.doi.org/10.1021/jp5050817 | J. Phys. Chem. C 2014, 118, 22553−22560

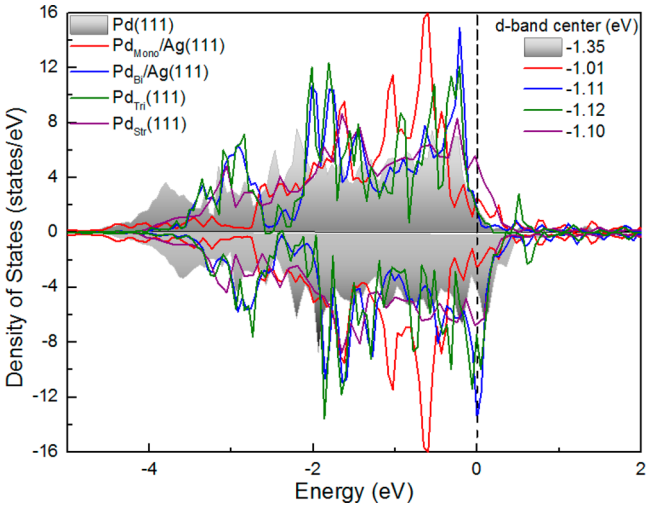

Figure 5. Projected density of states plots on the *d* states of pure Pd [indicated by Pd(111)], Pd monolayer supported on the Ag(111) substrate [Pd_{Mono}/Ag(111)], Pd bilayer on the Ag(111) substrate [Pd_{Bi}/Ag(111)], Pd trilayer on the Ag(111) substrate [Pd_{Tri}/Ag(111)], and 5.8% expansively strained Pd(111) surface [$Pd(111)_{Str}$]. The displayed dashed line at 0 eV stands for the Fermi level position. The slight mismatch between spin-up and spin-down states results from the nonzero magnetic moment. According to our DFT calculations, the Pd(111) surface yields the magnetic moment of 0.26 μ_B for a surface Pd atom, which is in good agreement with the previous study.[19]

energy) caused by the underlying Ag substrate. As a result of this opposite direction of ligand and strain effect, we see the noticeable reduction of adsorption energies of HCOO (E_{ad} = 0.14 eV) and HCO (0.22 eV) as compared to the pure Pd(111) surface, while for the CO/OH/H cases, the change of adsorption energy is insignificant, suggesting that the reduced activity of surface Pd atoms toward specific intermediates (especially, HCOO and HCO) may be responsible for the enhanced selectivity to H_2 production from HCOOH decomposition on the Pd_{Mono}/Ag(111) surface.

The decrease of adsorption energy in specific intermediates (HCOO and HCO) is related to the asymmetric modification of the activity of different surface sites by the interplay of ligand with strain effect and the difference of the site preference for the adsorption of intermediates. The relative contribution of strain and ligand effect on the change of adsorption energy in the Pd_{Mono}/Ag(111) surface with respect to the pure Pd (111) surface is shown in Table 3. Here, ΔE_{strain} is defined by $E_{ad}(Pd_{Str}/Ag(111)) - E_{ad}(Pd(111))$, which represents the stain contribution in surface adsorption process. While the calculated

Table 3. Relative Contribution of Strain and Ligand Effect in the Pd_{Mono}/Ag(111) Surface[a]

	strain contribution (ΔE_{strain})		ligand contribution (ΔE_{ligand})		combined contribution ($\Delta E_{total} = \Delta E_{strain} + \Delta E_{ligand}$)	
	hollow	top	hollow	top	hollow	top
HCOO	0.17	0.15	−0.12	−0.29	0.05	−0.14
CO	0.13	0.12	−0.13	−0.28	0	−0.16
HCO	0.16	0.06	−0.20	−0.26	−0.04	−0.20
OH	0.16	0.06	−0.16	−0.25	0	−0.19
H	0.10	−0.02	−0.09	−0.20	0.01	−0.22

[a] ΔE_{ligand}, [$=E_{ad}(Pd/Ag) - E_{ad}(Pd_{str})$] and ΔE_{strain} [$=E_{strain}(Pd_{Mono}/Ag(111)) - E_{ad}(Pd(111))$], which represent the ligand and strain contribution of Ag−Pd interaction to the adsorption energy of intermediates, respectively. The combined contribution [ΔE_{total}] is calculated by the sum of ΔE_{strain} and ΔE_{ligand}. The values are given in eV.

ΔE_{strain} values appear to correspond well to the d-band model, some adsorbate-site pairs, like the H adsorption at the top site with ΔE_{strain} = −0.02 eV, show deviations from the d-band model. Such an unexpected trend can be attributed to the modification of the local d-band by the presence of the adsorbate, although the d-band centers for clean Pd_{Mono}/Ag(111), Pd_{Bi}/Ag(111), Pd_{Tri}/Ag(111), and Pd_{Str}/Ag(111) surfaces are upshifted from the d-band center for the clean Pd(111) surface, as shown in Figure 5. In fact, the previous first-principles studies for the hydrogen adsorption on Pd(111) or Cu(111) revealed that at the top site, for symmetry reasons the hydrogen atom mainly interacts with only one d orbital [$d_{z^2-r^2}$ orbital] of the metal atom directly beneath, and the interaction is so strong that the d-band model is no longer fully appropriate.[23,24] Despite a rather fluctuating variation of ΔE_{strain} values, we find that at the top site of Pd atoms the ligand effect dominates the strain effect [note that ΔE_{strain} and ΔE_{ligand} is in the range of −0.02 ∼ +0.15 eV and −0.20 ∼ −0.29 eV, respectively], resulting in the reduction of adsorption energy [ΔE_{total} (ΔE_{strain} + ΔE_{ligand}) is in the range of −0.16 ∼ −0.22 eV], while at the hollow site, the strain and ligand almost cancel out each other [$|\Delta E_{total}| < 0.05$], leading to little change of adsorption energy. This result indicates that the ligand effect plays an important role in determining the activity of surface sites for the adsorption of intermediates. In particular, the top surface site is significantly affected by the ligand contribution. Together with the most favorable adsorption site of intermediates (the top site for HCOO/HCO and hollow site for CO/OH/H), this indicates the reduction of adsorption energy in HCOO/HCO and no variation in CO/OH/H (later,

Table 2. Adsorption Energies (E_{ad}) of the Key Intermediates (HCOO, H, HCO, OH, and CO) at the Most Favorable Adsorption Site on the Pure Pd [Pd(111)], Pd Monolayer on Ag(111) [Pd_{Mono}/Ag(111)], Pd Bilayer on Ag(111) [Pd_{Bi}/Ag(111)], Pd Trilayer on Ag(111) [Pd_{Tri}/Ag(111)], and Expansive-Strained Pd [Pd_{str} (111)] Surfaces[a]

	Pd_{Mono}/Ag(111)	Pd_{Bi}/Ag(111)	Pd_{Tri}(111)	Pd_{str}(111)	Pd(111)
E_{ad}(HCOO@top)/(ΔE_{ligand})	2.68(−0.29)	3.11(0.14)	2.98(0.01)	2.97(N/A)	2.82/(N/A)
E_{ad}(H@hollow)/(ΔE_{ligand})	2.65(−0.09)	2.80(0.06)	2.73(−0.01)	2.74(N/A)	2.64/(N/A)
E_{ad}(HCO@top)/(ΔE_{ligand})	1.64(−0.26)	2.02(0.12)	1.94(0.04)	1.90(N/A)	1.86/(N/A)
E_{ad}(OH@Hollow)/(ΔE_{ligand})	2.29(−0.16)	2.55(0.10)	2.49(0.04)	2.45(N/A)	2.29/(N/A)
E_{ad}(CO@hollow)/(ΔE_{ligand})	1.52(−0.13)	1.82(0.17)	1.70(0.05)	1.65(N/A)	1.52/(N/A)

[a] ΔE_{ligand}, which represent the ligand contribution of Ag−Pd interaction to the adsorption energy of HCOO, is defined as $E_{ad}(Pd/Ag) - E_{ad}(Pd_{str})$. The values are given in eV.

dx.doi.org/10.1021/jp5050817 | J. Phys. Chem. C 2014, 118, 22553−22560

Table 4. Bader Charge Gain or Loss ($\Delta\sigma$) at Each Level; The Negative and Positive Signs Refer to the Loss and Gain of Charge (in the Unit of e), Respectively

	Pd_{Mono}/Ag(111)	Pd_{Bi}/Ag(111)	Pd_{Tri}/Ag(111)	Pd_{Str}/(111)	Pd(111)
surface	0.388	0.118	0.124	0.129	0.108
subsurface	−0.348	0.142	−0.119	−0.109	−0.090
3rd layer	0.035	−0.260	−0.07	−0.08	−0.049

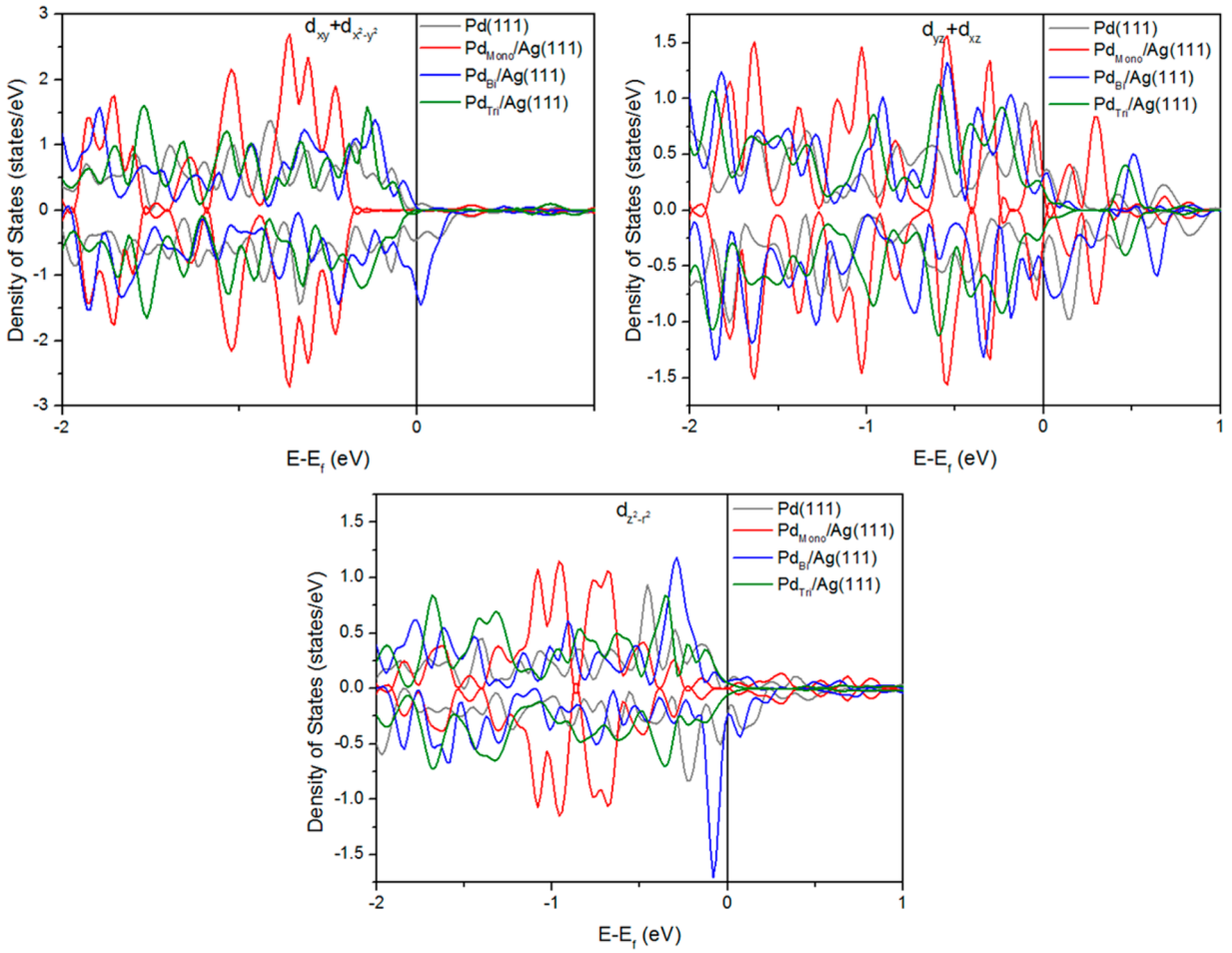

Figure 6. Orbital resolved density of states for *d* band; (a) $d_{xy} + d_{x^2-y^2}$; (b) $d_{xz} + d_{yz}$; (c) $d_{z^2-r^2}$. The displayed dashed line at 0 eV stands for the Fermi level position.

we will show the origin of the asymmetric modification of the activity of different surface sites by analyzing the electronic structure in detail).

In contrast, for the Pd_{Bi}/Ag(111) case, we see the positive values of ligand contribution in the range of 0.06−0.14 eV for the HCOO, HCO, OH, CO, and H, implying that the contribution of ligand effect to the adsorption energy is in the same direction as expansive strain contribution, resulting in the further increase of adsorption energies. The ligand contribution becomes almost negligible for the Pd_{Tri}/Ag(111) surface, and the adsorption energies on the Pd_{Tri}/Ag(111) surface hardly differ from those on the Pd_{Str}/Ag(111) surface. As a result, the adsorption energies of the key intermediates yield non-monotonic behaviors as a function of the number of Pd monolayers over Ag(111) with the maximum adsorption energies for the Pd_{Bi}/Ag(111) surface. These results indicate that if the Pd shell layer is as thin as one atomic layer, the Ag−Pd ligand effect dominates the strain effect and in turn significantly reduces the surface activity toward adsorbates.

This strong Ag−Pd ligand effect in the Pd_{Mono}/Ag(111) surface compared to the Pd_{Bi}/Ag(111) case is related to the modification of surface *d* band by the substantial charge distribution between surface Pd and subsurface Ag atoms. Table 4 displays the Bader charge gain or loss (indicated by $\Delta\sigma$) between interlayers at near surface on the bimetallic Pd/Ag systems. For the Pd_{Mono}/Ag(111) case, we find the significant increase in the electronic charge of surface Pd atom ($\Delta\sigma = 0.388e^-$) by the charge transfer from subsurface Ag atoms ($\Delta\sigma = -0.348e^-$), which is about three times higher than the surface Pd atom ($\Delta\sigma = 0.108\ e^-$) of the pure Pd(111) case. In contrast, for the Pd_{Bi}/Ag(111) ($\Delta\sigma = 0.118\ e^-$) and Pd_{Tri}/Ag(111) ($\Delta\sigma = 0.124\ e^-$) cases, we observe similar charge states of surface Pd atoms to the pure Pd(111) case.

Considering the significant disparities in the ligand contributions to the adsorption energies for the Pd_{Bi}/Ag(111) and Pd_{Tri}/Ag(111) surfaces, the differences in their the surface charge states and density of states appear to be rather modest. This indicates that a second-layer effect is responsible for the

dx.doi.org/10.1021/jp5050817 | J. Phys. Chem. C 2014, 118, 22553−22560

ligand contribution to the adsorption of intermediates on the $Pd_{Bi}/Ag(111)$ surface. In fact, previous first-principles studies have reported a second-layer effect for other bimetallic pseudomorphic overlayer systems such as Pd/Au(111) and Pt/Au(111), where the chemical bonding orbitals between the adsorbate and the first layer atoms overlap with the orbitals of the second layer atoms, resulting in the further increase of adsorption energies in addition to the strain constribution.[25] Overall, a combination of the strain effect, the charge transfer to the Pd surface from the subsurface Ag in the $Pd_{Mono}/Ag(111)$, and the second-layer effects in the $Pd_{Bi}/Ag(111)$ well accounts for the nonmonotonic variations of total energy changes and energy barriers in Table 1 as well as adsorption energies in Table 2 with respect to the number of Pd monolayers over the Ag(111) surface.

As a result of the striking difference in the surface charge states, we see the dramatic alteration of the LDOS of the $Pd_{Mono}/Ag(111)$ surface, in particular, the LDOS near the Fermi level (see Figure 5). Looking at the LDOS of the $Pd_{Bi}/Ag(111)$ and $Pd_{Tri}/Ag(111)$ surfaces, we find the high intensive peaks of the LDOS near the Fermi level (-0.5 eV $< E - E_f < 0$ eV). In contrast, for the $Pd_{Mono}/Ag(111)$ surface, we predict the significant reduction of the LDOS near the Fermi level (-0.5 eV $< E - E_f < 0$ eV). This absence of the LDOS near the Fermi level by the substantial charge transfer suggests the decrease of surface reactivity toward adsorbate. Note that at the condition of the strong ligand interaction in the bimetallic system, the catalytic surface having a lower density of state at the Fermi level tends to be less reactive in adsorption.[9,26]

In Figure 6, the orbital resolved density of states (ORDOS) for *d* orbitals are also displayed for further understanding how the activity of different surface sites (such as top and hollow) is asymmetrically affected by the Ag−Pd ligand interaction. First, for the $d_{xy} + d_{x^2-y^2}$ and $d_{z^2-r^2}$ cases, we see the large reduction of ORDOS near the Fermi level (-0.5 eV $< E - E_f < 0$ eV) on the $Pd_{Mono}/Ag(111)$ surface compared to the pure Pd(111) surface, while for the $Pd_{Bi}/Ag(111)$ and $Pd_{Tri}/Ag(111)$ surfaces we find the slight increase of ORDOS near the Fermi level. These results suggest the decrease in the surface activity of the $d_{xy} + d_{x^2-y^2}$ and $d_{z^2-r^2}$ orbitals toward adsorbate on the $Pd_{Mono}/Ag(111)$ surface, but the opposite is true for the $Pd_{Bi}/Ag(111)$ and $Pd_{Tri}/Ag(111)$ surfaces. On the other hand, for the $d_{xz} + d_{yz}$ case, we see no noticeable change of the ORDOS near the Fermi level on the three Pd overlayer surfaces compared to the pure Pd(111) case, indicating that the activity of the $d_{xz} + d_{yz}$ orbital on the $Pd_{Mono}/Ag(111)$, $Pd_{Bi}/Ag(111)$, and $Pd_{Tri}/Ag(111)$ surfaces is similar to the pure Pd(111) case. Considering that the $d_{z^2-r^2}$ and $d_{xz} + d_{yz}$ orbitals play an role in the adsorption at the top and hollow site, respectively (note that since the $d_{xy} + d_{x^2-y^2}$ orbitals lie in the $x-y$ plane, the contribution for adsorption process is relatively small compared to the $d_{z^2-r^2}$ and $d_{xz} + d_{yz}$ orbitals), these suggest that the Ag−Pd ligand effect plays an important role in determining the activity of different surface sites for the adsorption of intermediates. In particular, the activity of top site on the $Pd_{Mono}/Ag(111)$ case is significantly affected by the ligand contribution, while for the hollow site case the activity is little changed.

4. CONCLUSION

In this study, the DFT calculations have been performed to understand the importance of ligand effect on the bimetallic Pd/Ag catalysts in determining the HCOOH decomposition. For such purposes, we varied the number of Pd atomic layers at near surface. Our calculation revealed that the thickness of Pd atomic layers greatly affects the dehydrogenation and dehydration of HCOOH. In particular, the Pd monolayer significantly enhances the H_2 production from HCOOH by increasing the barrier of dehydrogenation and suppressing the dehydration barrier. The strong Ag−Pd ligand effect [which significantly reduces the density of state (especially, $d_{z^2-r^2}$ orbital) near the Fermi level] resulting from the charge transfer to the Pd surface from the subsurface Ag in the $Pd_{Mono}/Ag(111)$ surface substantially reduces the surface binding strength of specific intermediates, such as HCOO and HCO [note the insignificant change of adsorption energy for the other key intermediates (CO,OH and H)], which is responsible for the enhanced selectivity toward H_2 production from HCOOH decomposition. In contrast, the expansive (tensile) strain tends to decrease the selectivity to H_2 production. Our theoretical findings offer a plausible explanation on how the Ag−Pd core−shell catalysts boost the H_2 production activity from HCOOH decomposition and also provide a valuable insight into the modification of catalyst surface electronic properties, which is essential for a rational design of alloy catalysts.

■ ASSOCIATED CONTENT

Supporting Information

The intermediate images calculated during HCOOH decomposition on $Pd_{Bi}/Ag(111)$, $Pd_{Tri}/Ag(111)$, pure Pd(111), and $Pd(111)_{Str}$ and the calculated total energy changes and activation barriers for the 3 × 3 Pd/Ag slab cases are shown. This material is available free of charge via the Internet at http://pubs.acs.org.

■ AUTHOR INFORMATION

Corresponding Author

*E-mail: hchahm@kist.re.kr. Phone: +82-2-958-5889. Fax: +82-2-958-5199.

Notes

The authors declare no competing financial interest.

■ ACKNOWLEDGMENTS

The current work was financially supported by the New and Renewable Energy Core Technology Program of the Korea Institute of Energy Technology Evaluation and Planning (KETEP) granted financial resource from the Ministry of Trade, Industry & Energy, Republic of Korea (No. 20133030011320), and also supported by KIST institutional program for Korea Institute of Science and Technology. One of the authors (S.L.) wishes to acknowledge the financial support from the Basic Science Research Program through the National Research Foundation (NRF) of Korea funded by the Ministry of Education (NRF-2013R1A6A3A04059268) and the supercomputing resources from the Supercomputing Center/Korea Institute of Science and Technology Information (KSC-2013-C3-047).

■ REFERENCES

(1) (a) Ojeda, M.; Iglesia, E. Formic acid dehydrogenation on au-based catalysts at near-ambient temperatures. *Angew. Chem.* **2009**, *48* (26), 4800−3. (b) Haan, J. L.; Masel, R. I. The influence of solution pH on rates of an electrocatalytic reaction: Formic acid electro-oxidation on platinum and palladium. *Electrochim. Acta* **2009**, *54* (16), 4073−4078. (c) Lee, J. K.; Lee, J.; Han, J.; Lim, T. H.; Sung, Y. E.;

Tak, Y. Influence of Au contents of AuPt anode catalyst on the performance of direct formic acid fuel cell. *Electrochim. Acta* **2008**, *53* (9), 3474−3478. (d) Hu, S. Z.; Scudiero, L.; Ha, S. Electronic effect on oxidation of formic acid on supported Pd-Cu bimetallic surface. *Electrochim. Acta* **2012**, *83*, 354−358.

(2) Wang, G. M.; Morikawa, Y.; Matsumoto, T.; Nakamura, J. Why is formate synthesis insensitive to copper surface structures. *J. Phys. Chem. B* **2005**, *110*, 9.

(3) Boddien, A.; Loges, B.; Junge, H.; Gärtner, F.; Noyes, J. R.; Beller, M. Continuous hydrogen generation from formic acid: highly active and stable ruthenium catalysts. *Adv. Synth. Catal.* **2009**, *351* (14−15), 2517−2520.

(4) Yasaka, Y.; Yoshida, K.; Wakai, C.; Matubayashi, N.; Nakahara, M. Kinetic and Equilibrium Study on Formic Acid Decomposition in Relation to the Water-Gas-Shift Reaction. *J. Phys. Chem. A* **2006**, *110*, 11082.

(5) Cheng, X.; Shi, Z.; Glass, N.; Zhang, L.; Zhang, J.; Song, D.; Liu, Z.-S.; Wang, H.; Shen, J. A review of PEM hydrogen fuel cell contamination: Impacts, mechanisms, and mitigation. *J. Power Sources* **2007**, *165* (2), 739−756.

(6) Zhang, R.; Liu, H.; Wang, B.; Ling, L. Insights into the Preference of CO_2 Formation from HCOOH Decomposition on Pd Surface: A Theoretical Study. *J. Phys. Chem. C* **2012**, *116* (42), 22266−22280.

(7) Hu, C.; Pulleri, J. K.; Ting, S.-W.; Chan, K.-Y. Activity of Pd/C for hydrogen generation in aqueous formic acid solution. *Int. J. Hydrogen Energy* **2014**, *39* (1), 381−390.

(8) (a) Hu, C.; Ting, S.-W.; Chan, K.-Y.; Huang, W. Reaction pathways derived from DFT for understanding catalytic decomposition of formic acid into hydrogen on noble metals. *Int. J. Hydrogen Energy* **2012**, *37* (21), 15956−15965. (b) Kitchin, J.; Nørskov, J.; Barteau, M.; Chen, J. Role of Strain and Ligand Effects in the Modification of the Electronic and Chemical Properties of Bimetallic Surfaces. *Phys. Rev. Lett.* **2004**, *93*, 156801.

(9) Tedsree, K.; Li, T.; Jones, S.; Chan, C. W.; Yu, K. M.; Bagot, P. A.; Marquis, E. A.; Smith, G. D.; Tsang, S. C. Hydrogen production from formic acid decomposition at room temperature using a Ag-Pd core-shell nanocatalyst. *Nat. Nanotechnol.* **2011**, *6* (5), 302−7.

(10) Kresse, G.; Furthmuller, J. *VASP the Guide*; Vienna University of Technology: Vienna, Austria, 2001.

(11) Blochl, P. E. Projector augmented-wave method. *Phys. Rev. B* **1994**, *50* (24), 17953−17979.

(12) Blochl, P. E.; Jepsen, O.; Andersen, O. K. Improved tetrahedron method for brillouin-zone integrations. *Phys. Rev. B* **1994**, *49* (23), 16223−16233.

(13) Henkelman, G.; Uberuaga, B. P.; Jónsson, H. A climbing image nudged elastic band method for finding saddle points and minimum energy paths. *J. Chem. Phys.* **2000**, *113*, 9901.

(14) Hammer, B.; Hansen, L. B.; Norskov, J. K. Improved adsorption energetics within density-functional theory using revised Perdew-Burke-Ernzerhof functionals. *Phys. Rev. B* **1999**, *59* (11), 7413−7421.

(15) (a) Markovic, N. M.; Ross, P. N. Surface science studies of model fuel cell electrocatalysts. *Surf. Sci. Rep* **2002**, *45* (4−6), 121−229. (b) Lu, G. Q.; Crown, A.; Wieckowski, A. Formic acid decomposition on polycrystalline platinum and palladized platinum electrodes. *J. Phys. Chem. B* **1999**, *103* (44), 9700−9711. (c) Macia, M. D.; Herrero, E.; Feliu, J. M. Formic acid oxidation on Bi-Pt(111) electrode in perchloric acid media. A kinetic study. *J. Electroanal. Chem.* **2003**, *554*, 25−34. (d) Capon, A.; Parsons, R. Oxidation of formic-acid at noble-metal electrodes 0.1. review of previous work. *J. Electroanal. Chem.* **1973**, *44* (1), 1−7. (e) Park, S.; Wieckowski, A.; Weaver, M. J. Electrochemical infrared characterization of CO domains on ruthenium-decorated platinum nanoparticles. *J. Am. Chem. Soc.* **2003**, *125* (8), 2282−2290.

(16) (a) Neurock, M.; Janik, M.; Wieckowski, A. A first principles comparison of the mechanism and site requirements for the electrocatalytic oxidation of methanol and formic acid over Pt. *Faraday Discuss.* **2008**, *140*, 363−378. (b) Chen, Y. X.; Heinen, M.; Jusys, Z.; Behm, R. J. Kinetic isotope effects in complex reaction networks: Formic acid electro-oxidation. *ChemPhysChem* **2007**, *8* (3), 380−385.

(17) (a) Wilhelm, S.; Iwasita, T.; Vielstich, W. COH and CO as adsorbed intermediates during methanol oxidation on platinum. *J. Electroanal. Chem.* **1987**, *238* (1−2), 383−391. (b) Xia, X. H.; Iwasita, T. Influence of underpotential deposited lead upon the oxidation of HCOOH in $HClO_4$ at platinum-electrodes. *J. Electrochem. Soc.* **1993**, *140* (9), 2559−2565.

(18) Bulushev, D. A.; Beloshapkin, S.; Ross, J. R. H. Hydrogen from formic acid decomposition over Pd and Au catalysts. *Catal. Today* **2010**, *154* (1−2), 7−12.

(19) Chepulskii, R. V.; Barabash, S. V.; Zunger, A., Ab initio theory of phase stability and structural selectivity in Fe-Pd alloys. *Phys. Rev. B* **2012**, *85* (14).

(20) Mavrikakis, M.; Hammer, B.; Nørskov, J., Effect of Strain on the reactivity of metal surfaces. *Phys. Rev. Lett.* **1998**, *81*.

(21) Maark, T. A.; Peterson, A. A. Understanding strain and ligand effects in hydrogen evolution over Pd(111) surfaces. *J. Phys. Chem. C* **2014**, *118* (8), 4275−4281.

(22) Ham, H. C.; Manogaran, D.; Lee, K. H.; Kwon, K.; Jin, S. A.; You, D. J.; Pak, C.; Hwang, G. S., Communication: Enhanced oxygen reduction reaction and its underlying mechanism in Pd-Ir-Co trimetallic alloys. *J. Chem. Phys.* **2013**, *139* (20).

(23) Sakong, S.; Gross, A. Dissociative adsorption of hydrogen on strained Cu surfaces. *Surf. Sci.* **2003**, *525* (1−3), 107−118.

(24) Roudgar, A.; Gross, A., Local reactivity of metal overlayers: Density functional theory calculations of Pd on Au. *Phys. Rev. B* **2003**, *67* (3).

(25) Gohda, Y.; Gross, A. Structure-reactivity relationship for bimetallic electrodes: Pt overlayers and PtAu surface alloys on Au(111). *J. Electroanal. Chem.* **2007**, *607* (1−2), 47−53.

(26) Tong, Y. Y.; Yonezawa, T.; Toshima, N.; vanderKlink, J. J. Pt-195 NMR of polymer-protected Pt/Pd bimetallic catalysts. *J. Phys. Chem.* **1996**, *100* (2), 730−733.